Proceedings of the 17th World Congress
The International Federation of Automatic Control
Seoul, Korea, July 6-11, 2008

Optimal State Space Control of DC Motor

M. Ruderman, J. Krettek, F. Hoffmann, T. Bertram

Chair for Control Systems Engineering, Technische Universität Dortmund, D-44221 Germany (Tel. +49/231/755-2496, e-mail: mykhaylo.ruderman@tu-dortmund.de)

Abstract:
In comparison to classical cascade control architecture of DC motors, the state feedback control offers advantages in terms of design complexity, hardware realization and adaptivity. This paper presents a methodic approach to state space control of a DC motor. The state space model identified from experimental data provides the basis for a linear quadratic regulator (LQR) design. The state feedback linear control is augmented with a feedforward control for compensation of Coulomb friction. The controller is successfully applied and the closed loop behavior is evaluated on the experimental testbed under various reference signals.

Keywords: model-based control; LQR control method, motor control; state-space models; feedforward compensation

1. INTRODUCTION

DC motors provide an attractive alternative to AC servo motors in high-performance motion control applications. DC motors are in particular popular in low-power and high precise servo applications due to their reasonable cost and ease of control. Traditionally motor controls in industrial applications employ a cascade control structure. The outer speed and inner current control loops are designed as PD or PI controllers. However, the cascaded control structure assumes that the inner loop dynamics are substantially faster than the outer one (Chevrel et al. (1996)).

In recent years several publications propose alternative approaches to identification and control of DC motors. Umeno and Hori (1991) describe a generalized speed control design technique of DC servomotors based on the parametrization of two-degrees-of-freedom controllers and apply the design method of a Butterworth filter to determine the controller parameter. Chevrel et al. (1996) present a switched LQR speed controller, designed from the linear model of the DC motor, and compare its performance with a cascade control design in terms of accuracy, robustness and complexity. Rubaai and Kotaru (2000) propose an alternative way to identify and control DC motors by means of a nonlinear control law represented by an artificial neural network. Yu and Hwang (2004) present an LQR approach to determine the optimal PID speed control of the DC motor.

This contribution proposes a systematic approach to velocity controller design of a DC motor based on model identification and LQR design augmented with a nonlinear feedforward compensator. The electrical and mechanical parameters of the DC motor, i.e., resistance, inertia, back-EMF, damping are identified from observations of the open loop response. Coulomb friction is considered as the main cause of the nonlinear motor behavior and is adequately compensated by a feedforward control signal. The residual steady state error caused by minor nonlinearities and uncertainties in the model is compensated by an integral error feedback signal. The proposed controller is evaluated for high and low velocity reference profiles including velocity reversal to demonstrate its efficiency for high-performance servo applications. The proposed scheme attempts to bridge the current gap between the advance of control theory and the practice of DC actuator systems.

This paper is structured as follows: Section 2 describes the state-space model of the DC motor derived from electromechanical relationships including friction. The model identification is described in Section 3. Section 4 details the LQR design of the optimal state feedback control with an integrator and the feedforward friction compensation. Section 5 analyzes the closed performance on the experimental testbed under different velocity reference profiles. Finally, Section 6 summarizes the major conclusions of the paper.

2. DC MOTOR MODEL

2.1 Linear state-space model

Under the assumption of a homogenous magnetic field, the direct current (DC) motor is modeled as a linear transducer from motor current to electrical torque. The classical model of the DC motor, described by Isermann (2002) is composed of a coupled electrical and a mechanical subsystem.

The angular velocity ω is controlled by the input voltage u with a constant voltage drop attributed to the brush and rotor resistance, and a back-electromotive force (EMF) caused by the rotary armature. The motor inductance contributes proportional to the change in motor current i. The motor current couples the electrical component with the mechanical one, as it generates the driving torque. This torque is antagonized by the motor inertia,

structure damping, friction, and the external load. The motor dynamics are described by:

$$u(t) = L\,\frac{di}{dt} + R_m\,i(t) + K_e\,\omega(t)\,, \tag{1}$$

$$K_m\,i(t) = J\,\frac{d\omega}{dt} + K_d\,\omega(t) + \tau_l + \tau_f\,, \tag{2}$$

where K_m, K_e and K_d denote the motor torque, the back-EMF and the damping constants. J denotes the mechanical inertia including the motor armature and shaft. L and R_m represent the inductance and the total connection resistance of the motor. The system load and friction are denoted by τ_l and τ_f.

However, for many applications this structure is not sufficient. The main drawback of the linear state-space model is a negligence of nonlinear effects, whose properties can significantly affect the dynamic behavior of a modeled system. To complete the representation of essential physical phenomena effecting in the motor structure the frictional nonlinearity must be included.

2.2 System nonlinearity

According to Paduart et al. (2006)) the linear state-space model with a multivariable nonlinear input function $f(\mathbf{x}(t), u(t))$ assumes the general form:

$$\dot{\mathbf{x}} = \mathbf{A}\,\mathbf{x} + \mathbf{B}\,u + \mathbf{H}\,f(\mathbf{x}, u)\,, \tag{3}$$

in which $\mathbf{A}$ is the system matrix, $\mathbf{B}$ is the input vector, and the coupling vector $\mathbf{H}$ links the nonlinearity with the linear part. In context of permanent magnet DC motor Coulomb friction constitutes the major source of nonlinear behavior (Knudsen and Jensen (1995)). Additional nonlinearities emerge from the inhomogeneity of the stator magnetic field and transfer characteristics of the amplifier and IO elements as well as motor cogging and ripple effects (see Proca et al. (2003)).

Tjahjowidodo et al. (2005) describe advanced friction models which introduce auxiliary internal states to capture friction dynamics. As these auxiliary states are not observable customized identification techniques are required for the identification of their associated parameters. For many applications a static friction model that includes Coulomb and viscous parts suffices to capture the main frictional phenomena.

The linear viscous friction is already comprehended in the damping term in equation (2). Considering the nonlinear Coulomb friction which depends on the rotation direction and introducing the state vector $\mathbf{x} = [i,\,\omega]^T$ results in:

$$\dot{\mathbf{x}} = \begin{bmatrix} -\frac{R_m}{L} & -\frac{K_e}{L} \\ \frac{K_m}{J} & -\frac{K_d}{J} \end{bmatrix} \mathbf{x} + \begin{bmatrix} \frac{1}{L} \\ 0 \end{bmatrix} u + \begin{bmatrix} 0 \\ -\frac{F_c}{J} \end{bmatrix} \operatorname{sgn}(x_2) \tag{4}$$

in which F_c denotes the Coulomb friction coefficient. The overall model has six independent parameters, of which the inductance $L = 25 \times 10^{-6}$ H is obtained from the manufacturer datasheet and the remaining five parameters are identified from experimental data.

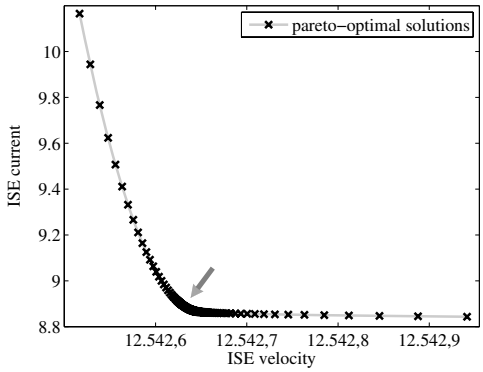

Fig. 1. Pareto-optimal compromises between ISE for current and angular velocity

3. MODEL IDENTIFICATION

The signals for identification are generated from the open loop step response of the DC motor at different amplitudes. The identification yields the set of optimal parameters that minimize the squared error between model output and data.

$$\begin{aligned} E_\omega &= \int (\omega(t) - \hat{\omega}(t))^2 dt \\ E_i &= \int (i(t) - \hat{i}(t))^2 dt\,. \end{aligned} \tag{5}$$

As the model is linear in the unknown parameters, these are identified by means of least squares. The remaining choice is the trade-off between the two errors. This trade-off is specified by their relative weight w in

$$E = wE_\omega + (1 - w)E_i\,. \tag{6}$$

In the context of state feedback control the model should not only reflect the input-output behavior but also accurately describe the dynamics of internal states, in our case the motor current.

Fig. 1 visualizes the set of pareto-optimal solutions obtained from variations of the weight $w \in [0, 1]$. The squared error in the angular velocity is rather insensitive to parameter variations as the stick slip effect at low velocities causes an oscillation in the angular velocity (see upper left graph in Fig. 2) not captured by the model. This deviation causes a large offset in squared error compared which the residual error contributions in the rising edge and steady state are negligible. The compromise solution is marked by an arrow in Fig. 1.

The actual step responses are compared with the model output in Fig. 2 for a subset of six out of sixteen signals taken into account for identification. The graphs show that the identified parameters correctly capture the steady state behavior as well as the characteristic time constants in the rising edge. The oscillatory behavior at low frequencies does not correspond to an eigen frequency of the system but merely reflects the variation of friction during a complete rotation of the motor shaft.

The identified parameters are listed in Table 1 and compared with the nominal values provided by the manufacturer. The differences between the nominal and the iden-

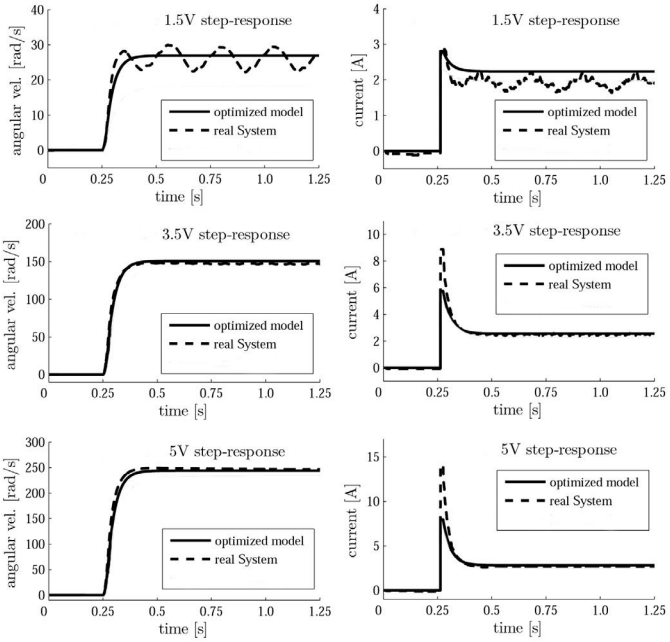

Fig. 2. Comparison of real and model step-responses for velocity and current at different voltages

tified inertia and friction are explained by the additional inertia and bearing of the rotary encoder. The increase of identified resistance is explained by additional contacts of the motor connection and structure changes of the motor brushes and commutator. The other identified parameters are in accordance with the nominal values.

Table 1. System parameter identification

	nominal	*identified*
total motor resistance R_m (Ω)	0.35	0.98
torque constant K_m (N m/A)	0.0296	0.0274
EMF constant K_e (V s/rad)	0.0296	0.0297
damping constant K_d (N s/rad)	6.7×10^{-5}	7.2×10^{-5}
total system inertia J (kg m^2)	2.9×10^{-6}	3.2×10^{-5}
Coulomb friction F_c (N m)	0.0200	0.0593
inductance L (H)	25×10^{-6}	

4. CONTROL DESIGN

State feedback controller design is accomplished either by pole placement or in the context of optimal control by means of linear quadratic regulator (LQR) design (see Anderson and Moore (2007)). In pole placement the designer specifies the desired eigenvalues of the closed loop system in the left half plane. LQR design minimizes a weighted squared state error and control effort. The optimal feedback state regulation, minimizes the quadratic cost function

$$J = \int_0^\infty \left(\mathbf{x}^T(t) \mathbf{Q}\, \mathbf{x}(t) + \mathbf{u}^T(t) \mathbf{R}\, \mathbf{u}(t) \right), \tag{7}$$

in which $\mathbf{Q}$ and $\mathbf{R}$ are symmetric, positive semi-definite respectively positive definite weight matrices. The optimal feedback gain

$$\mathbf{K} = \mathbf{R}^{-1} \mathbf{B}^T \mathbf{P}, \tag{8}$$

is obtained from the solution $\mathbf{P}$ of the algebraic Riccati equation:

$$\mathbf{A}^T \mathbf{P} + \mathbf{P}\mathbf{A} - \mathbf{P}\mathbf{B}\mathbf{R}^{-1}\mathbf{B}^T\mathbf{P} + \mathbf{Q} = 0\,. \tag{9}$$

The weight matrices are specified such that the closed loop system is able to track the reference signal with a control signal that does not significant violates the saturated actuator limits. For a fixed weight matrix $\mathbf{Q}$, the control penalty R is chosen such that for the maximum state error, the feedback control signal

$$u = -\mathbf{K}\mathbf{x} + V\omega_r \tag{10}$$

is in accordance with the actuator bounds. To compensate the steady state error of the closed control loop a feedforward term is included in the control:

$$V = -(\mathbf{C}^T(\mathbf{A} - \mathbf{B}\mathbf{K})^{-1}\mathbf{B})^{-1}\,. \tag{11}$$

To compensate disturbances, and model uncertainties of the DC model the integral output error

$$\varepsilon = \int_0^t (\omega_r - \omega_a)\, dt \tag{12}$$

is introduced as an additional state variable, in which ω_r and ω_a denote the reference and actual velocities. The linear part of the state space model is augmented by the auxiliary integral state variable:

$$\begin{bmatrix} \dot{\mathbf{x}} \\ \dot{\varepsilon} \end{bmatrix} = \begin{bmatrix} \mathbf{A} & 0 \\ -\mathbf{C}^T & 0 \end{bmatrix} \begin{bmatrix} \mathbf{x} \\ \varepsilon \end{bmatrix} + \begin{bmatrix} \mathbf{B} \\ 0 \end{bmatrix} u + \begin{bmatrix} 0 \\ 1 \end{bmatrix} \omega_r\,. \tag{13}$$

Correspondingly the weight matrix is augmented with a small weight for the integral error.

$$\mathbf{Q} = \begin{bmatrix} 1 & 0 & 0 \\ 0 & 1 & 0 \\ 0 & 0 & 0.001 \end{bmatrix}, \quad R = 10\,. \tag{14}$$

4.1 Feedforward friction compensation

The closed loop behavior is further improved by a feedforward control for immediate compensation of Coulomb friction. The friction is constant and it sign is opposite to the direction of rotation. The discontinuity at velocity reversal is smoothed by replacing the step at $\omega_r = 0$ by a linear segment for small velocities in the range of $\sigma = \pm 1$ rad/s. The add-on feedforward control gain

$$K_f = \frac{R_m\, F_c}{K_m}\,, \tag{15}$$

determined from equations (1) and (2) by the elimination of all dynamic terms compensates the static friction phenomenon.

Table 2. Controller parameters

friction gain K_f	1.06
feedforward gain V	0.3166
feedback gain K_i	0.0984
feedback gain K_ω	0.3003
feedback gain K_ε	-0.01

4.2 Control law

The overall control law including feedforward compensation

$$\Gamma = \begin{cases} K_f \operatorname{sgn}(\omega_r), & if \quad |\omega_r| > \sigma \\ K_f \dfrac{\omega_r}{\sigma}, & else \end{cases} \tag{16}$$

becomes

$$u = -[\mathbf{K}_{i,\omega}\ K_\varepsilon] \begin{bmatrix} \mathbf{x} \\ \varepsilon \end{bmatrix} + [\Gamma\ V] \begin{bmatrix} 1 \\ \omega_r \end{bmatrix}, \tag{17}$$

with the corresponding gains listed in Table 2.

The entire control structure in state space representation is depicted in Fig. 3.

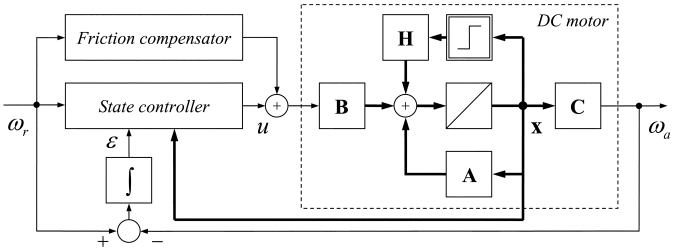

Fig. 3. Block diagram: proposed control structure with a state-space system representation

5. CONTROL SYSTEM BEHAVIOR

5.1 Disturbance rejection

The designed velocity controller is validated on the nominal model in simulation for different reference signals. To analyze the robustness of the controller an external periodic disturbance torque with amplitude of 0.06 Nm and pulse width 0.01 s is applied to motor. The disturbance has the same magnitude as the constant DC motor friction.

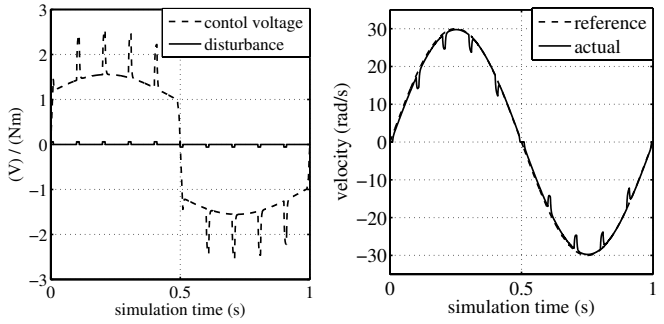

Fig. 4. Simulation results: torque disturbance and control voltage (left), reference and actual velocity (right)

The controller responds immediately to the disturbance resulting in a rapid compensation of the error in output velocity as shown in Fig. 4. Notice, that the designed controller is specifically adopted to the unloaded operation of the DC motor. The identification and control system design has to be repeated if the DC motor is utilized to drive an permanent external load. If the applied load is not known in advance, an adaptive control scheme is advocated.

5.2 Experimental setup

The experimental testbed of the DC motor for identification and control is shown in Fig. 5. The sample rate of the real time controller onboard the host computer is 5 kHz. The control signal u_{out} with a range of ±5 V applied to the DC motor is amplified. The motor is an AXEM DC servo motor with a shrunk-on-disk rotor, F9M2 with rated power output of 63 W and rated speed 3000 r.p.m. (=314.1593 rad/s).

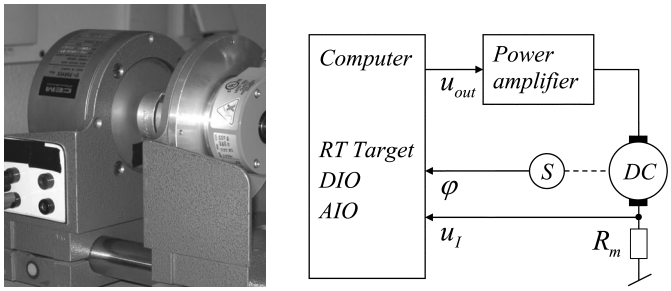

Fig. 5. Laboratory testbed: DC motor with a rotary encoder (left), and system overview (right)

The motor current is measured by the voltage drop u_I across a shunt R_m, and the motor shaft position φ and direction of rotation are provided by a digital single turn rotary encoder S with 13 bit resolution. The angular velocity is obtained from time derivation of the shaft position. A low pass filter with window size 3 is applied to smooth the velocity signal and reduce the quantization errors.

5.3 Velocity control

The tracking behavior of the velocity controller is evaluated for a sinusoidal signal with amplitude of 200 rad/s and period of 0.4 s and a sequence of up and down step signals with reference velocities in the absolute range of 5 up to 220 rad/s at intervals of 0.4 s.

The reference and observed velocities as well as simulated response of the closed loop system are depicted in Fig. 6 a) and b). The controller is able to track the reference signal and with no residual steady state error at high as well as low velocities. The closed loop system exhibits a lag characteristic with a time constant determined by the slowest eigenvalue attributed to the mechanical subsystem. To recognize is the overlap in acceleration phase of the closed loop behavior and the open loop response (by saturated control signal) depicted in Fig. 6 c), which indicates a maximal achievable controller performance bounded by actuator properties. Plotting the signals from Fig. 6 at larger scale in Fig. 7 reveals that the actual velocity oscillates with small amplitude around the reference velocity. This jitter is caused by the limited resolution of the rotary encoder. The amplitude of the jitter corresponds to the magnitude equivalent to a single bit and is independent of progress of the angular velocity.

The control signal saturates during the acceleration and deceleration phases, such that the ability to track the reference is effectively dominated by the actuator limitations rather than the control. Fig. 8 compares the observed current with the current predicted by the model in case of step

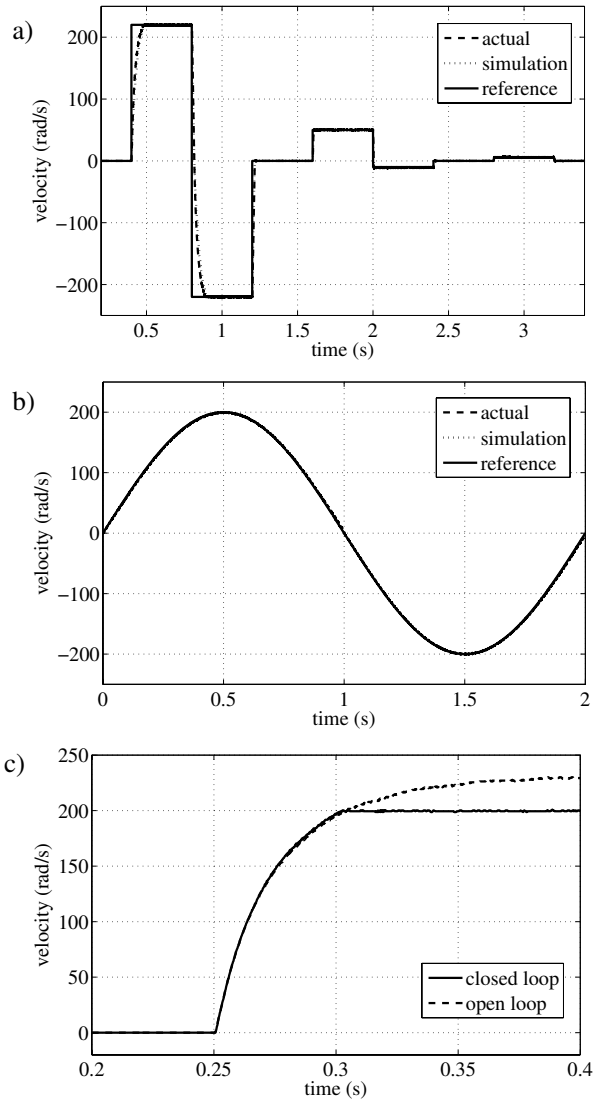

Fig. 6. Experimental results: a) stair shaped signal, b) sinusoidal signal, c) step response of the open and closed loops

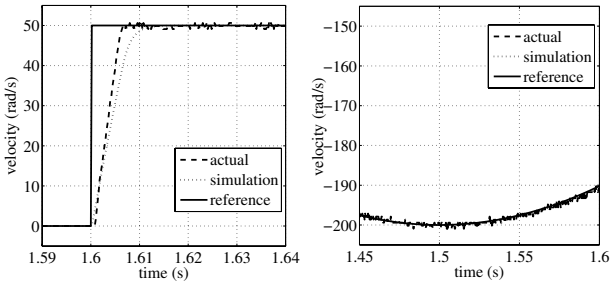

Fig. 7. Zoom in of angular velocity

responses. The current peaks in case of abrupt changes in reference velocities causing large state errors. The actual peak currents are about two to three times larger than the predicted ones whereas the steady state currents match. We assume that the excess in peak currents is explained by the initial breakaway force (static friction) that the motor has to overcome. Nevertheless, these peaks are not critical as the maximal allowed motor current of 60 A is not exceeded. The high-frequency jitter of the current signal at steady state is attributed to the cogging and ripple effects and the stick-slip motion.

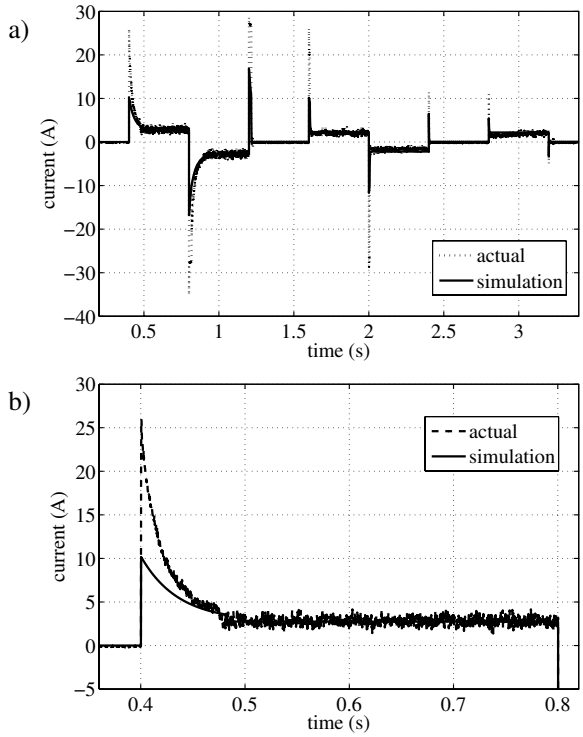

Fig. 8. Model predicted and measured motor current by the stair shaped reference signal a) and zoom in of motor current b)

6. CONCLUSIONS

This paper proposes a novel approach to control design of a DC servomotor based on system identification and LQR control design. The feedback controller is augmented with a feed-forward friction compensation. The mechanical and electrical parameters of the DC motor are identified from the open loop responses with respect to motor current and angular velocity. The LQR design provides an optimal state feedback control minimizes the quadratic state error and control effort. The auxiliary integral error state and feedforward compensation of the nonlinear friction reduce the residual error across the entire range of reference velocities. The experimental results demonstrate the feasibility of the controller design for high precision servo applications. The proposed method is well suited for the controller design of highly dynamic DC motors. Future research is concerned with the design of adaptive controllers to handle variations of load and the identification of periodical disturbances and advanced friction models.

ACKNOWLEDGEMENTS

The authors are grateful to the Kübler GmbH company for providing the sensor. We also thank Heiko Preckwinkel for controller implementation and experiments.

REFERENCES

B. D. O. Anderson and J. B. Moore. *Optimal Control: Linear Quadratic Methods.* Dover Publications, 2007.

P. Chevrel, L. Sicot, and S. Siala. Switched LQ controllers for DC motor speed and current control: acomparison with cascade control. In *Proc. Power Electronics Specialists Conference PESC'96 Record.*, pages 906–912, Baveno, Italy, June 1996.

R. Isermann. *Mechatronische Systeme*. Springer, Berlin, 2002.

M. Knudsen and J. G. Jensen. Estimation of nonlinear DC-motor models using a sensitivity approach. In *Proc. 3. European Control Conference ECC'95*, Rome, Italy, 1995.

J. Paduart, J. Schoukens, K. Smolders, and J. Swevers. Comparison of two different nonlinear state-space identification algorithms. In *Proc. International Conference on Noise and Vibration Engineering ISMA'06*, Leuven, Belgium, September 2006.

A. B. Proca, A. Keyhani, A. El-Antably, W. Lu, and M. Dai. Analytical model for permanent magnet motors with surface mounted magnets. *IEEE transactions on energy conversion*, 18:386–391, 2003.

A. Rubaai and R. Kotaru. Online identification and control of a DC motor using learning adaptation of neural networks. *IEEE transactions on industrial applications*, 36:935–942, 2000.

T. Tjahjowidodo, F. Al-Bender, and H. Van Brussel. Friction identification and compensation in a DC motor. In *Proc. 16th IFAC World Congress*, Prague, Czech Republic, July 2005.

T. Umeno and Y. Hori. Robust speed control of DC servomotors using modern two degrees-of-freedom controller design. *IEEE Transactions on industrial electronics*, 38: 363–368, 1991.

G.-R. Yu and R.-C. Hwang. Optimal PID speed control of brush less DC motors using LQR approach. In *Proc. IEEE International Conference on Man and Cybernetics*, pages 473–478, Hague, Netherlands, October 2004.